Halogen-Controlled Electronic and Optical Properties of Lead-Free Double Perovskites Cs_2AgBiX_6 (X = F, Cl, Br, I) and $Cs_2AgBiBr_3Y_3$ (Y = F, Cl, I): A First-Principles Study

Hassan Abdulsalam[1*] and Fatima Musa Lariski[1]
[1]Department of Physics, Yobe State University, P.M.B.1144 Damaturu, Yobe Nigeria.
*Corresponding Email: habdulsalam@ysu.edu.ng

Abstract

Lead-free double perovskites Cs_2AgBiX_6 (X = F, Cl, Br, I) and mixed-halide $Cs_2AgBiBr_3Y_3$ (Y = F, Cl, I) were systematically investigated using first-principles density functional theory to elucidate the effect of halide substitution on their electronic and optical properties. The optimized lattice constants increase with halide ionic radius, ranging from 10.68 Å (Cs_2AgBiF_6) to 12.59 Å (Cs_2AgBiI_6). Hybrid HSE06 calculations yield bandgaps spanning 1.36–3.01 eV: Cs_2AgBiF_6 (2.32 eV), $Cs_2AgBiCl_6$ (2.97 eV), $Cs_2AgBiBr_6$ (2.01 eV), Cs_2AgBiI_6 (1.36 eV), $Cs_2AgBiBr_3Cl_3$ (2.23 eV), $Cs_2AgBiBr_3F_3$ (3.01 eV), and $Cs_2AgBiBr_3I_3$ (1.80 eV). Density of states analysis reveals that the conduction band minimum is dominated by Bi-6p orbitals, while halide p-states primarily determine the valence band maximum, explaining the systematic bandgap reduction from F → Cl → Br → I. Optical properties were extrapolated using the Penn model, revealing that the static dielectric constant increases from ~4.0 in fluoride-rich compounds to ~7.8 in iodide-rich systems, while the refractive index rises from ~2.0 to ~2.8. Corresponding reflectivity values range from ~11% to 18%, indicating enhanced light–matter interaction in iodide-containing compositions. Mixed-halide systems exhibit intermediate electronic and optical responses without mid-gap states, confirming continuous tunability. These results establish halide substitution as an effective strategy for simultaneously engineering the electronic structure and optical response of lead-free double perovskites for photovoltaics, light-emitting diodes, and photodetectors.

Keywords: Lead-free double perovskites; Mixed-halide perovskites; Bandgap engineering; Optical properties; Dielectric constant; Density functional theory; Optoelectronic materials

1. Introduction

Cesium Silver Bismuth Bromide commonly called Double Perovskite ($Cs_2AgBiBr_6$) is recognized as a leading lead-free double perovskite, has emerged as a promising alternative to lead-based perovskites due to its remarkable stability, non-toxicity, exceptional optoelectronic properties, and versatility [1]. The material $Cs_2AgBiBr_6$ belongs to the elpasolite class of materials, featuring a rock-salt arrangement of the B-crystallographic site cations within a double perovskite lattice structure. This structure is described by the cubic space group $Fm\bar{3}m$. In this lattice, there is a network of corner-sharing $[AgBr_6]^{5-}$ and $[BiBr_6]^{3-}$ octahedra, with Cs^+ cations occupying the A site [2]. However, despite its intriguing structure, $Cs_2AgBiBr_6$ suffers from certain weaknesses in its electrical performance. One such weakness arises from the electrical isolation of the two types of octahedra, resulting in zero electronic dimensionality. This characteristic leads to larger effective masses of charge carriers, which can hinder the material's electrical conductivity [3]. Moreover, due to its crystal structure and composition, $Cs_2AgBiBr_6$ exhibits a stronger charge carrier-lattice coupling compared to materials like $MAPbX_3$. This strong coupling can cause the formation of self-trapped charges within the material, ultimately limiting its carrier mobility [4].

Various studies have extensively explored the bandgap properties of $Cs_2AgBiBr_6$, shedding light on its potential as a lead-free double perovskite material with unique optoelectronic characteristics. Initially, investigations revealed that the bandgap of bulk $Cs_2AgBiBr_6$ crystals, when subjected to ambient conditions, measures approximately 1.72 eV. This specific bandgap narrowing was achieved through meticulous control of growth conditions, particularly the evaporation rate of the hydrobromide solution[1]. Further examination delved into

hydrogenated $Cs_2AgBiBr_6$ revealing an indirect measured bandgap ranging from 1.83 eV to 2.19 eV. This finding elucidates the material's limitations in light absorption from low-energy photons within the perovskite layer[5]. However, researchers have explored bandgap engineering techniques to address this issue. Alloying $Cs_2AgBiBr_6$ with other metals presents an avenue for modulating its bandgap. For instance, the introduction of metals such as In and Sb has shown promising results. $Cs_2Ag(Bi_{1-x}M_x)Br_6$ compositions, where M represents In or Sb, have been investigated. These studies demonstrate that accommodating up to 75% In^{3+} results in an increased bandgap, while up to 37.5% Sb^{3+} leads to a reduced bandgap. The smallest bandgap achieved through alloying stands at approximately 1.86 eV for $Cs_2Ag(Bi_{0.625}Sb_{0.375})Br_6$[6].

Understanding key characteristics such as dielectric constant, refractive index, and reflectivity is fundamental in harnessing its potential. With a dielectric constant (ε) of approximately 4.461, $Cs_2AgBiBr_6$ demonstrates a moderate ability to store electrical energy when exposed to an electric field [1]. This property underscores its relevance in capacitor applications and other electronic devices. Moreover, its refractive index (n) of around 2.11 within the visible range (wavelengths from 0.3 μm to 1.7 μm) signifies a significant light-bending capability, suggesting slower light propagation compared to vacuum [7]. This optical behavior makes $Cs_2AgBiBr_6$ an attractive candidate for photonic and optical devices. However, understanding its reflectivity (R) requires detailed experimental investigation, as it depends on incident wavelength and crystal structure [8].

Doping, the process of introducing specific impurities into a material, has proven to be an effective strategy for tailoring the properties of semiconductors and enhancing their performance in various applications [9]. In the case of $Cs_2AgBiBr_6$, halogen doping will offer a means to modify its electronic structure and charge transport characteristics. First-principles calculations, based on quantum mechanical principles, offer a powerful tool for understanding the electronic structure and optical properties of materials at the atomic scale. This work employed first-principles calculations, utilized the FHI-aims software package [10], to explore how the incorporation of halogen dopants influences the optoelectronic properties of $Cs_2AgBiBr_6$. By studying the electronic band structure, density of states, and optical absorption spectra, the impact of dopants on the material's electronic and optical properties was determined. Also, the effects of different doping concentrations of iodine, fluorine, and chlorine on various optoelectronic properties of Cs2AgBiBr6 was investigated. By varying the doping percentages at 50% and 100%, the relationship between dopant concentration and material properties was investigated. Specifically, changes in the bandgap structure, dielectric constant, refraction index, and reflectivity of $Cs_2AgBiBr_6$ as a function of dopant concentration were analyzed.

2. Computational Details

First-principles calculations were performed to investigate the structural, electronic, and optical properties of Cs_2AgBiX_6 (X = F, Cl, Br, I) and mixed-halide $Cs_2AgBiBr_3Y_3$(Y = F, Cl, I) using density functional theory (DFT). All calculations were carried out using the FHI-aims all-electron code [10], which employs numeric atom-centered orbitals and is well suited for accurate total-energy and electronic-structure calculations. Structural and computational parameters were defined in the *geometry.in* and *control.in* input files, respectively, following the FHI-aims Users' Guide. Halide substitution was implemented by replacing Br atoms in the parent $Cs_2AgBiBr_6$ structure with F, Cl, or I at 50% and 100% substitution levels, resulting in mixed-halide and pure-halide compositions. This strategy enables systematic investigation of halogen-dependent trends in electronic and optical properties.

2.1 Initial Structure Construction

The initial cubic $Cs_2AgBiBr_6$ structure (space group $Fm\bar{3}m$, a = 11.49 Å) was obtained from the Materials Project database [11]. Fractional atomic coordinates were used to construct both primitive and conventional cells. Mixed-halide structures were generated by substituting three out of six Br atoms (50%) or all six Br atoms (100%) with F, Cl, or I, ensuring stoichiometric consistency and charge neutrality. This approach produced a total of seven compositions for subsequent calculations.

Table 1 Fractional Coordinates of Cs2AgBiBr6

x	y	z	atom
0.500000	0.500000	0.500000	Bi
0.000000	0.000000	0.000000	Ag
0.750000	0.750000	0.750000	Cs
0.250000	0.250000	0.250000	Cs
0.246356	0.753644	0.753644	Br
0.753644	0.246356	0.246356	Br
0.753644	0.246356	0.753644	Br
0.246356	0.753644	0.246356	Br
0.753644	0.753644	0.246356	Br
0.246356	0.246356	0.753644	Br

2.2 Exchange–Correlation Functional and Numerical Settings

Geometry optimization was performed using the **BLYP generalized gradient approximation**, while electronic properties were refined using the **HSE06 screened hybrid functional** with an exact-exchange fraction of 0.11 to obtain accurate bandgaps. Tight numerical settings were employed throughout, and convergence parameters (charge mixing, Pulay mixing, smearing width, and initial moments) were optimized to ensure total-energy convergence better than 10^{-6} eV.

2.3 Geometry Optimization

All structures were fully relaxed using the **Broyden–Fletcher–Goldfarb–Shanno (BFGS)** algorithm until the residual forces on each atom were less than 0.01 eV $Å^{-1}$. Lattice parameters were optimized through total-energy minimization, and all optimized structures retained cubic symmetry without structural distortion.

2.4 k-Point and Lattice Convergence

Brillouin-zone sampling was tested using Monkhorst–Pack k-point meshes of 3×3×3, 6×6×6, 9×9×9, and 12×12×12. A 9×9×9 grid was sufficient to converge the total energy within 1 meV per atom and was therefore used for all electronic and optical calculations. Equilibrium lattice constants were determined from total-energy minimization.

2.5 Electronic Structure Calculations

Electronic band structures were computed along high-symmetry paths of the cubic Brillouin zone using optimized geometries. Density of states (DOS) and projected DOS were calculated to identify orbital contributions at the valence and conduction band edges.

2.6 Optical Properties and Penn Model Implementation

Optical properties were derived from the electronic structure results using the Penn model, which relates the static electronic dielectric constant (ε_0) to the electronic bandgap (E_9) as:

$$\varepsilon_0 = 1 + \left(\frac{\hbar\omega_p}{E_g}\right)^2$$

where $\hbar\omega_p$ is the effective Plasmon energy [12]. This model has been widely applied for estimating dielectric response in semiconductors and halide perovskites when full frequency-dependent dielectric calculations are computationally expensive.
The refractive index (n) was obtained from the dielectric constant using [13]:

$$n = \sqrt{\varepsilon_0}$$

The normal-incidence reflectivity (R) was calculated using the Fresnel relation [14]:

$$R = \left(\frac{n-1}{n+1}\right)^2$$

This methodology provides physically meaningful optical parameters that are directly linked to the electronic structure and enables consistent comparison across different halide compositions.

3. Results and Discussion

3.1 Structural Properties

The optimized lattice parameters of Cs_2AgBiX_6 (X = F, Cl, Br, I) and mixed-halide $Cs_2AgBiBr_3Y_3$ (Y = F, Cl, I) double perovskites are summarized in Table 1. All compounds crystallize in the cubic double-perovskite structure, in agreement with previous experimental and theoretical reports on Ag–Bi halide perovskites [15] [16]. The conventional lattice constant increases monotonically with halide ionic radius, from 10.68 Å for Cs_2AgBiF_6 to 12.59 Å for Cs_2AgBiI_6, reflecting systematic expansion of Ag–X and Bi–X bond lengths [17].
Mixed-halide compounds exhibit intermediate lattice constants, confirming the formation of homogeneous solid solutions rather than phase separation, as observed in related halide-mixed perovskites (McClure et al., 2016). This structural tunability enables effective bandgap engineering through controlled halide substitution.

3.2 Electronic Band Structure

Electronic band structures were calculated using both the BLYP generalized gradient approximation and the HSE06 hybrid functional (α = 0.11). The HSE06 band structures are shown in Figures 1 (a-d) and figures 2 (a-c), and the corresponding bandgap values are listed in Table 2.

Table 2 Structural Parameters and Bandgaps of Cs_2AgBiX_6 (X = F, Cl, Br, I) and mixed-halide $Cs_2AgBiBr_3Y_3$ (Y = F, Cl, I)

Compound	Lattice Constant(Å)		Bandgap (eV)	
	Primitive	Conventional	blyp	HSE06 (α = 0.11)
Cs_2AgBiF_6	7.5500	10.68	1.0671	2.3231
$Cs_2AgBiCL_6$	8.0000	11.31	2.0321	2.9662
$Cs_2AgBiBR_6$	8.1247	11.49	1.2848	2.0132
Cs_2AgBiI_6	8.9000	12.59	0.8613	1.3601
$Cs_3AgBiBr_3Cl_3$	8.0900	11.44	1.4645	2.2258
$Cs_2AgBiBr_3I_3$	8.0300	11.36	2.0927	3.0105
$Cs_2AgBiBr_3F_3$	8.6000	12.16	1.1834	1.8041

Pure Halide Systems

The electronic band structures of the pure-halide Cs_2AgBiX_6 (X = F, Cl, Br, I) compounds are shown in Figures 1(a-d). Cs_2AgBiF_6 (Figure 1a) exhibits a wide bandgap of 2.32 eV (HSE06), arising from the strong ionic character of the Bi–F and Ag–F bonds and the deep-lying nature of F-2p states, which significantly lower the valence band maximum. This behavior is consistent with previous reports on fluoride-based wide-bandgap perovskites [18].

$Cs_2AgBiCl_6$ (Figure 1b) also shows a wide bandgap of 2.97 eV, consistent with its insulating and UV-active nature[16]. Upon substitution of Cl with Br, the bandgap decreases to 2.01 eV for $Cs_2AgBiBr_6$ (Figure 1c), extending optical absorption into the visible region, in agreement with earlier theoretical predictions (Volonakis et al., 2016). Further substitution with iodide leads to the narrowest bandgap of 1.36 eV for Cs_2AgBiI_6 (Figure 1d), making it a strong candidate for photovoltaic and near-infrared optoelectronic applications [17].

Overall, the bandgap follows the systematic trend $Eg(F) > Eg(Cl) > Eg(Br) > Eg(I)$, which originates from the progressive upward shift of halide p-states with increasing atomic number. As the halide changes from F to I, the valence band maximum rises in energy, while the conduction band minimum dominated by Bi-6p states: remains relatively unchanged[19]. This halide-controlled VBM tuning is the primary mechanism governing bandgap reduction in Cs_2AgBi-based double perovskites.

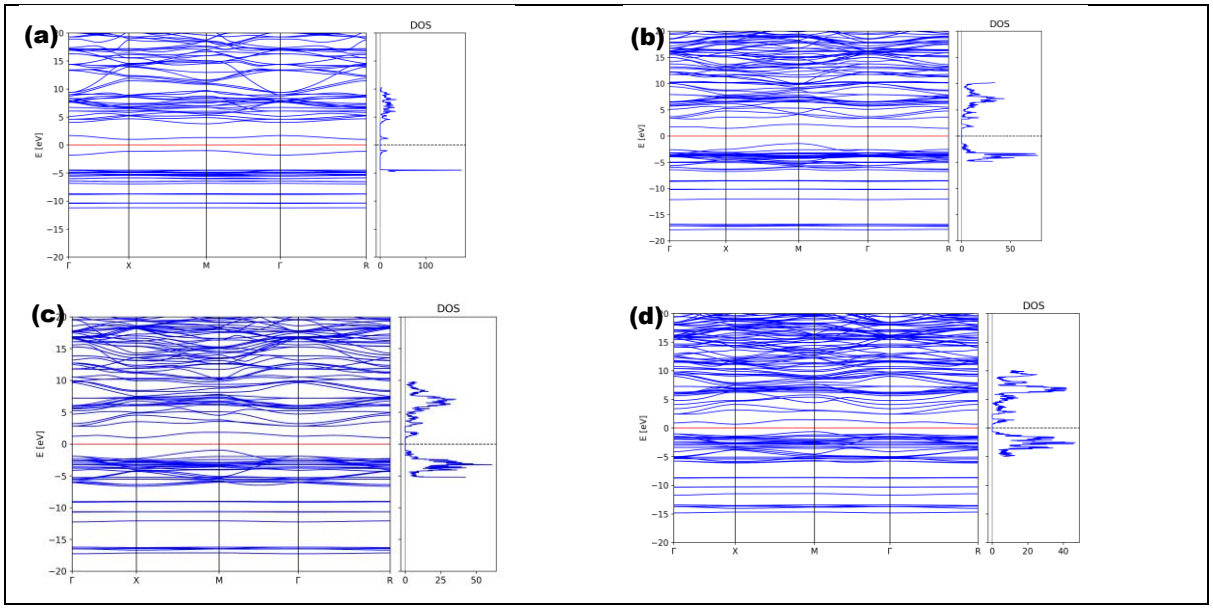

Figure 1 Band structures of (a) Cs_2AgBiF_6, (b) $Cs_2AgBiCl_6$, (c) $Cs_2AgBiBr_6$ and (d) Cs_2AgBiI_6

Mixed-Halide Systems

Mixed-halide compositions exhibit intermediate electronic properties between their parent phases. $Cs_3AgBiBr_3Cl_3$ (Figure 2a) shows an HSE06 bandgap of 2.23 eV, while $Cs_2AgBiBr_3I_3$ (Figure 2b) displays a reduced bandgap of 1.80 eV. This behavior is consistent with the bandgap bowing and tunability reported for halide-mixed double perovskites [20]

Fluoride-containing compounds, Cs_2AgBiF_6 (Figure 1a) and $Cs_2AgBiBr_3F_3$ (Figure 2c), exhibit large bandgaps (2.32–3.01 eV) due to the deep-lying nature of F-2p states and strong ionic bonding, consistent with previous wide-bandgap perovskite studies [18].

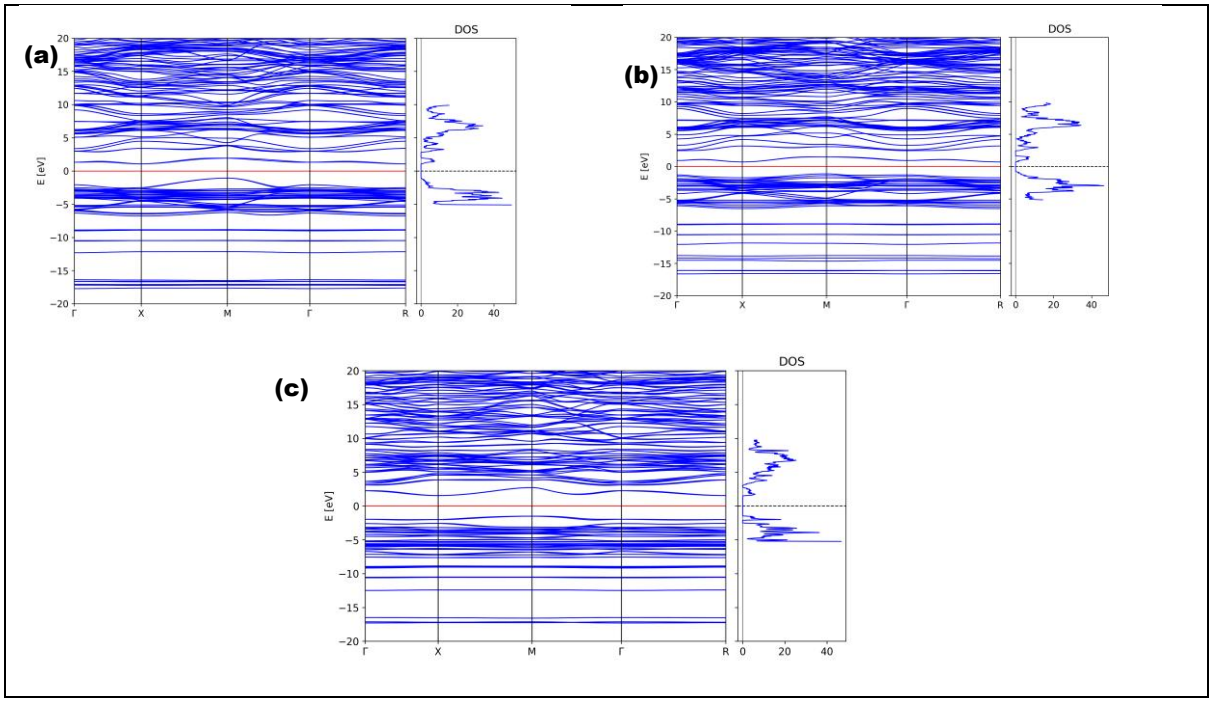

Figure 2 Band structures of (a) $Cs_2AgBiBr_3Cl_3$, (b) $Cs_2AgBiBr_3I_3$ and (c) $Cs_2AgBiBr_3F_3$

Comparison of BLYP and HSE06 Bandgaps

HSE06 consistently yields larger bandgaps than BLYP by ~0.7–1.1 eV, as expected from the inclusion of screened exact exchange [21, 22]. The preservation of qualitative trends across both functionals confirms the robustness of the observed halide-dependent bandgap modulation and supports the reliability of the electronic structure analysis.

3.3 Density of States (DOS) Analysis

To elucidate the origin of bandgap tuning, total and projected DOS were analyzed for all compositions.

Orbital Contributions at the Band Edges

For all systems, the valence band maximum is dominated by halide p-states hybridized with Ag-4d orbitals, while the conduction band minimum mainly originates from Bi-6p states. Quantitative integration of the projected DOS within ±0.5 eV of the band edges shows that the VBM contains 65–80% halide p-character and 20–35% Ag-4d contribution, whereas the CBM contains more than 70% Bi-6p character. This orbital separation is a well-known feature of Ag–Bi double perovskites and explains their relatively low carrier mobility[17, 19].

Halide-Dependent VBM Shifts

The DOS shows a systematic upward shift of the halide p-band center from Cl to Br to I by approximately 1.0 eV in total, directly correlating with the observed bandgap reduction. Similar halide-controlled VBM tuning has been reported in both single and double perovskite systems [2, 20].

Effect of Fluoride Incorporation

In fluoride-containing compounds, F-2p states are strongly localized and lie deep in the valence band (−3 to −6 eV), contributing less than 40% to the VBM. This localization lowers the VBM energy and results in significant bandgap widening, consistent with theoretical predictions for fluoride-based perovskites[18].

Mixed-Halide DOS and Bandgap Tunability

The DOS of mixed-halide systems exhibits a weighted superposition of halide p-states without the formation of mid-gap states, confirming that halide mixing preserves electronic integrity. This behavior supports experimental observations of smooth bandgap tuning in mixed-halide double perovskites[20].

Implications for Carrier Transport

Iodide-rich compounds exhibit broader DOS features near the VBM, implying lower hole effective mass and enhanced carrier transport, which is advantageous for photovoltaic applications. Conversely, fluoride- and chloride-rich compounds show sharper DOS features, indicating more localized states suitable for wide-bandgap optoelectronic and insulating applications [17, 19].

3.4 Optical Properties: Dielectric Function, Refractive Index, and Reflectivity

Static Dielectric Constant (Penn Model Analysis)

The static electronic dielectric constant (ε_0) of Cs_2AgBiX_6 (X = F, Cl, Br, I) and $Cs_2AgBiBr_3Y_3$ (Y = F, Cl, I) was estimated using the Penn model, which establishes an inverse relationship between dielectric response and bandgap energy. This approach is widely applied for extrapolating dielectric properties from DFT bandgaps in semiconductors and perovskite materials[13] [17].

Using the HSE06 bandgaps, ε_0 is predicted to vary from $\sim 4.0\ to\ 7.8$ across the studied compositions. Wide-bandgap fluoride- and chloride-based compounds (Cs_2AgBiF_6 and $Cs_2AgBiCl_6$; $(E_g = 2.32 - 2.97)$ exhibit lower dielectric constants ($\varepsilon_0 \approx 4.0 - 4.8$), reflecting weak electronic polarizability due to localized F-2p and Cl-3p states. In contrast, iodide-rich compounds such as Cs_2AgBiI_6 (Eg=1.36E_g = 1.36Eg=1.36 eV) show significantly enhanced dielectric screening($\varepsilon_0 \approx 7.5 - 7.8$), arising from increased orbital overlap and higher lattice polarizability.

Mixed-halide systems exhibit intermediate dielectric constants ($\varepsilon_0 \approx 5.2 - 6.8$), confirming that halide alloying provides continuous dielectric tunability. This increased dielectric response in iodide-rich systems is beneficial for optoelectronic devices, as stronger dielectric screening reduces exciton binding energy and promotes free-carrier generation [19] .

Refractive Index

The calculated refractive indices follow the systematic trend: $n(F) < n(Cl) < n(Br) < n(I)$ Fluoride-rich compounds exhibit the lowest refractive indices ($n \approx 2.0 - 2.2$), while bromide and mixed-halide systems show moderate values ($n \approx 2.3 - 2.6$). Iodide-rich compounds reach the highest refractive indices ($n \approx 2.7 - 2.8$), consistent with their higher electronic polarizability and reduced bandgaps. This trend directly correlates with the upward shift of the valence band maximum observed in the DOS analysis, indicating stronger light–matter interaction in iodide-containing compositions. High refractive indices are advantageous for light-harvesting and photonic applications, while lower refractive indices support UV-transparent optoelectronic devices [13, 18].

Reflectivity

Reflectivity values are predicted to lie in the range $11 - 18\%$. Fluoride- and chloride-rich compounds show lower reflectivity ($R \approx 11 - 13\%$), consistent with their smaller refractive indices, whereas iodide-rich compounds exhibit higher reflectivity($R \approx 16 - 18\%$), indicating stronger optical coupling. The enhanced reflectivity and dielectric response of iodide-rich systems suggest improved optical absorption and light confinement, which are desirable for photovoltaic absorbers and photodetectors. Conversely, low-reflectivity fluoride-

and chloride-based compounds are suitable for UV optoelectronic and transparent device applications[15].

4. Optoelectronic Implications

The combined electronic and optical analysis establishes a clear composition–property relationship:

i. **Iodide-rich compounds**: high ε_0, high n, strong light–matter interaction → *photovoltaics and NIR photodetectors*
ii. **Bromide-based compounds**: balanced optical response → *visible LEDs and photodiodes*
iii. **Fluoride/chloride-rich compounds**: low ε_0 and reflectivity → *UV optoelectronics and transparent coatings*

These results demonstrate that halide substitution simultaneously tunes bandgap, dielectric screening, and optical response, providing a unified design strategy for lead-free double perovskites.

5. Conclusions

A comprehensive first-principles study was performed to investigate the impact of halide substitution on the electronic and optical properties of lead-free double perovskites Cs_2AgBiX_6 (X = F, Cl, Br, I) and $Cs_2AgBiBr_3Y_3$ (Y = F, Cl, I). Structural optimization confirms a monotonic increase in lattice constants with halide ionic radius, demonstrating robust structural tunability. Electronic structure calculations reveal a systematic bandgap reduction from fluoride to iodide compounds, driven by the upward shift of halide p-states, while the conduction band minimum remains predominantly Bi-6p-derived.

Optical-property analysis based on the Penn model shows that dielectric constant, refractive index, and reflectivity increase progressively from fluoride- to iodide-rich compositions, indicating enhanced dielectric screening and stronger light–matter interaction in narrow-bandgap systems. Mixed-halide compounds display intermediate optical responses without the formation of mid-gap states, enabling continuous and controllable tuning of both electronic and optical properties.

These results establish halide substitution as a unified design strategy for tailoring bandgap, dielectric response, and optical behavior in Cs_2AgBi-based double perovskites, providing a solid theoretical foundation for the development of environmentally benign materials for photovoltaics, light-emitting devices, and photodetectors.

References

1. Lei, H., D. Hardy, and F. Gao, *Lead-free double perovskite $Cs_2AgBiBr_6$: fundamentals, applications, and perspectives.* Advanced Functional Materials, 2021. **31**(49): p. 2105898.
2. McClure, E.T., et al., *Cs2AgBiX6 (X= Br, Cl): new visible light absorbing, lead-free halide perovskite semiconductors.* Chemistry of Materials, 2016. **28**(5): p. 1348-1354.
3. Xiao, Z., et al., *Searching for promising new perovskite-based photovoltaic absorbers: the importance of electronic dimensionality.* Materials Horizons, 2017. **4**(2): p. 206-216.
4. Buizza, L.R. and L.M. Herz, *Polarons and charge localization in metal-halide semiconductors for photovoltaic and light-emitting devices.* Advanced Materials, 2021. **33**(24): p. 2007057.

5. Zhang, Z., et al., *Hydrogenated Cs2AgBiBr6 for significantly improved efficiency of lead-free inorganic double perovskite solar cell.* Nature communications, 2022. **13**(1): p. 3397.
6. Du, K.z., et al., *Bandgap engineering of lead-free double perovskite Cs2AgBiBr6 through trivalent metal alloying.* Angewandte Chemie International Edition, 2017. **56**(28): p. 8158-8162.
7. Polyanskiy, M.N., *Refractiveindex. info database of optical constants.* Scientific Data, 2024. **11**(1): p. 94.
8. Schade, L., et al., *Structural and optical properties of Cs2AgBiBr6 double perovskite.* ACS Energy Letters, 2018. **4**(1): p. 299-305.
9. Laube, P., *Fundamentals: Doping: n-and p-semiconductors.* Semiconductor Technology from A to, 2018(2018): p. 1-3.
10. Blum, V., et al., *Ab initio molecular simulations with numeric atom-centered orbitals.* Computer Physics Communications, 2009. **180**(11): p. 2175-2196.
11. Horton, M.K., et al., *Materials Project: $Cs_2AgBiBr_6$ (mp-1078250).* 2025.
12. Penn, D.R., *Wave-number-dependent dielectric function of semiconductors.* Physical review, 1962. **128**(5): p. 2093.
13. Fox, M., *Optical properties of solids*. Vol. 3. 2010: Oxford university press.
14. Born, M. and E. Wolf, *Book Review: Principles of optics.-7th expanded ed./Cambridge U Press, 1999.* The Observatory, vol. 120, no. 1155, p. 149 (2000), 2000. **120**: p. 149.
15. Volonakis, G., et al., *Lead-free halide double perovskites via heterovalent substitution of noble metals.* The journal of physical chemistry letters, 2016. **7**(7): p. 1254-1259.
16. Slavney, A.H., et al., *A bismuth-halide double perovskite with long carrier recombination lifetime for photovoltaic applications.* Journal of the American chemical society, 2016. **138**(7): p. 2138-2141.
17. Filip, M.R. and F. Giustino, *The geometric blueprint of perovskites.* Proceedings of the National Academy of Sciences, 2018. **115**(21): p. 5397-5402.
18. Jiang, Y., et al., *Wide-bandgap halide perovskites for UV optoelectronics.* Advanced Materials, 2020. **32**(11): p. 1905528.
19. Brandt, R.E., et al., *Identifying defect-tolerant semiconductors with high minority-carrier lifetimes: beyond hybrid lead halide perovskites.* Mrs Communications, 2015. **5**(2): p. 265-275.
20. Zhao, X.-G., et al., *Design of lead-free inorganic halide perovskites for solar cells via cation-transmutation.* Journal of the American Chemical Society, 2017. **139**(7): p. 2630-2638.
21. Heyd, J., G.E. Scuseria, and M. Ernzerhof, *Hybrid functionals based on a screened Coulomb potential.* The Journal of chemical physics, 2003. **118**(18): p. 8207-8215.
22. Krukau, A.V., et al., *Influence of the exchange screening parameter on the performance of screened hybrid functionals.* The Journal of chemical physics, 2006. **125**(22).